ACS APPLIED ENGINEERING MATERIALS

pubs.acs.org/acsaenm Article

Upcycled Polyvinyl Chloride (PVC) Electrospun Nanofibers from Waste PVC-Based Materials for Water Treatment

Atta Ur Razzaq, D. J. McEachern, Paul A. Rupar, Phoebe R. Willis, S. Nima Mahmoodi, and Milad Rabbani Esfahani*

Cite This: ACS Appl. Eng. Mater. 2023, 1, 1924–1936 Read Online

ACCESS | Metrics & More | Article Recommendations | Supporting Information

ABSTRACT: In recent decades, the increased use of polyvinyl chloride (PVC) in industries and households has led to a surge in PVC waste pollution, which mandates developing solutions for the removal of waste PVC from the environment. We report upcycling, the conversion of waste material to a high-value-added product, of PVC-based products to electrospun (ES) fibers (mats). As two common PVC products, waste PVC pipe and waste PVC pool float were upcycled to ES fibers for water treatment. The fabrication process and fiber characteristics, such as morphology, surface charge, and mechanical strength of upcycled fibers, were studied and compared with the same fibers fabricated using research-grade (RG) PVC (commercial PVC powder). In addition, the effect of additives such as calcium carbonate in PVC waste products on the physicochemical properties of upcycled fibers was evaluated. The results showed that upcycling of waste PVC to ES fibers is feasible since the upcycled fibers showed similar or superior properties compared to their equivalent fibers from RG-PVC. Finally, the performance of upcycled fibers on the removal of dyes from the water was evaluated. The upcycled fibers from waste PVC pipes and pool float outperformed the RG PVC fibers in removing methylene blue from water by showing more than 97% removal efficiency. In addition, the upcycled PVC ES fibers showed more than 80% reusability after five adsorption−desorption cycles.

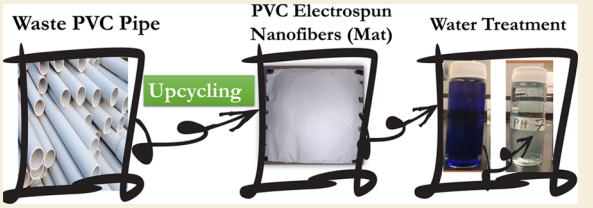

KEYWORDS: *plastic pollution, adsorption, clean environment, wastewater treatment*

1. INTRODUCTION

Synthetic polymers have been widely used in various commercial and household applications since the 1940s because of their low cost, light weight, corrosion resistance, and processability.[1,2] Due to the slow biodegradation of plastics, their accumulation in the environment is fast, which causes several environmental problems. Currently, there are different disposal and treatment methods, such as landfill disposal, incineration, and plastic recycling, as solutions for the plastic pollution problems.[2] However, there are a few challenges with each of these methods. For instance, the primary purpose of recycling is to remake and reuse the same plastics and not to change their life cycle,[3−5] incineration of plastic waste is harmful to the environment,[6] and landfilling leads to the accumulation of different plastics and occupies a lot of space.[7] A better method for dealing with plastic pollution is upcycling.[2] Upcycling is defined as the process of converting low-cost wastes into high-performance fuels, chemicals, and materials (new polymers, composite materials, membranes, and nanofibers) by extracting the embedded value present in the form of carbon, hydrogen, chemical, energy, or macromolecular structure.[8] Upcycling processes may provide novel approaches to dealing with real-world plastic wastes, particularly those that cannot be recycled thermomechanically. As a result, there is no doubt that upcycling plastic waste would contribute to the reduction of solid waste contamination while also producing high-value products, implying significant economic and scientific opportunities.[8]

Polyvinyl chloride (PVC) is a thermoplastic material that is widely used in different applications such as pipes, packaging materials, window frames, cables, bottles, and even in medical devices due to its advantageous physical, chemical, and anti-degradable properties such as high mechanical strength, durability, excellent resistance to acids and bases, and low production costs.[9−13] PVC is the second most-produced thermoplastic after polyethylene.[9,14] In 2015, 38 million tons of PVC were produced, and 16 million tons of PVC waste was generated.[15]

Electrospun (ES) technology has evolved into one of the most widely used methods for producing high-quality nanofiber material/mats for applications in water treatment.[16,17] The advantages of ES technology include simple manufacturing devices, low spinning costs, a diverse range of spinnable

Received: May 10, 2023
Revised: May 29, 2023
Accepted: May 30, 2023
Published: June 27, 2023

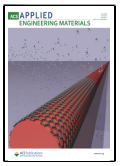

https://doi.org/10.1021/acsaenm.3c00245
ACS Appl. Eng. Mater. 2023, 1, 1924−1936

materials, and precise and controllable processes.[16] ES nanofibers have extraordinary properties, such as enhanced porosity, high flux, energy efficiency, a well-interconnected network, significant internal surface area, a three-dimensional fibrous system, and exceptional separation ability, making them suitable to remove various pollutants from water.[16,17] A few studies reported the fabrication of micro- and nanofibers from waste plastics using electrospinning. For instance, nanofibers were successfully electrospun from pure polyethylene terephthalate (PET), polystyrene (PS), and polycarbonate (PC), and it was concluded that the mechanical properties of the nanofibers generated from the mixed waste of the three polymers were superior to those of the commercial polymers with the same molecular weight.[18] In another study, nanofibrous membranes were successfully electrospun from waste PET, PS, and PC, where the effect of changing electrospinning parameters, such as the applied voltage and needle diameter, had on the properties of the final materials, such as fiber diameters and fiber distribution, was reported.[19,20] Upcycling plastics to high-added-value products is a promising approach but needs more experimental and practical results to show the capability of current approaches and their pros and cons.

In this paper, we studied upcycling waste PVC pipe and PVC pool float to the high value-added product of ES nanofibers for water treatment. The waste PVC was acquired from a plumbing pipe and a pool float and was transformed into ES fibers using the electrospinning method. We systematically investigated the electrospinning fabrication process and the resulting physicochemical properties of ES fibers, such as morphology, fiber diameters, surface chemistry, surface charge, and mechanical stability and benchmarked them with ES fibers fabricated using research-grade (RG) PVC. In addition, we investigated the effect of $CaCO_3$, a common additive to PVC pipe and pool float, on the properties of ES fibers. Finally, we examined the performance of the upcycled ES fibers (mat) to remove methylene blue (MB) dye from water. The main advantage of reported upcycled fibers as the adsorbents is that they were synthesized using "waste" PVC plastic. Therefore, they have a low material cost. Also, they showed comparable performance in terms of adsorption percentage and adsorption capacity compared with the other ES adsorbents reported in the literature (Table 2).

2. MATERIALS AND METHODS

2.1. Materials

Waste PVC pipes and PVC pool float were collected from the landfill directly. The RG PVC powder ($M_w \sim 50{,}000$ g/mol and $M_n \sim 35{,}000$ g/mol) was purchased from Sigma-Aldrich (Milwaukee, WI, United States). Calcium carbonate ($CaCO_3$) was purchased from Fisher Scientific (New Jersey, United States). Tetrahydrofuran (THF) (purity, ≥99.9%) was purchased from Honeywell-Burdick & Jackson (Muskegon, MI, United States). *N*,*N*-Dimethylformamide (DMF) (purity, ≥99.9%), hydrochloric acid, and potassium chloride (KCl) were purchased from VWR (Suwanee, GA, United States) and sodium hydroxide (NaOH) was purchased from BeanTown Chemical (BTC) (Hudson, United States). MB ($C_{16}H_{18}ClN_3S{\cdot}H_2O$, λ = 665 nm) was purchased from Merck (Darmstadt, Germany).

2.2. Sample Pretreatment

After water washing the collected waste PVC pipes, they were soaked in acetone for softening and cutting. The pipe was then cut into small pieces with an average size of (*L*: 1.19, *W*: 0.94, *H*: 0.386 cm) and then, the samples were left to dry for 1 week, allowing all the acetone to evaporate. The pieces were then washed with deionized water and dried at room temperature. No pretreatment was done for the PVC pool float, and they were only cut into smaller pieces (*L*: 1.32, *W*: 1.01, *H*: 0.029 cm).

2.3. Preparation of the Casting Solution

Six different casting solutions were prepared by dissolving an appropriate amount of (1) PVC pipe, (2) PVC pool float, (3) RG PVC, (4) a mixture of 3 wt % $CaCO_3$ and 12 wt % RG (3%-$CaCO_3$-RG), (5) a mixture of 8 wt % $CaCO_3$ and 7 wt % RG (8%-$CaCO_3$-RG) in THF and DMF in a volume ratio of 2 to 3, respectively. Sample 3 was chosen as the control to be compared with both waste-PVC samples. Samples 4 and 5 were designed to study the effect of $CaCO_3$ and polymer content ratio in comparison to waste-PVC and RG-PVC samples. One separate casting solution (sample 6) was prepared by centrifuging the PVC pipe casting solution and separating the supernatant. For the preparation of the casting solution of samples 1, 2, and 3, 15 wt % of the PVC pipe, PVC pool float, and RG PVC were used. Since the commercial PVC pipe and pool float possess $CaCO_3$ as an additive, samples 4 and 5 were prepared using RG PVC with 3 and 8% $CaCO_3$ to examine the effect of $CaCO_3$ on the upcycled ES fibers. To investigate the impact of soluble and insoluble components of commercial PVC, sample 6 was prepared by centrifuging the casting solution of the PVC pipe at 4000 rpm for 90 min using an Eppendorf Centrifuge 5810 machine. The supernatant was separated from the precipitate and used as a casting solution for electrospinning. All the casting solutions were prepared by stirring at 400 rpm at 23 °C for 19 h. The casting solutions were degassed for 4 h before electrospinning.

2.4. Electrospinning Parameters

All six casting solutions were electrospun under the same conditions using a horizontal electrospinning setup (Figure 1). A 12 mL plastic

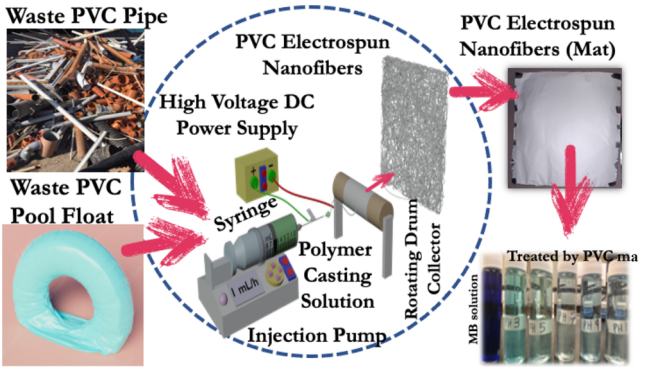

Figure 1. Roadmap of the upcycling process of PVC waste materials, which consists of PVC pipes and PVC pool float converted to ES nanofibers for water treatment (dye removal). The schematic illustrates the horizontal electrospinning setup that consists of a syringe (12 mL), needle (19 gauge), high-voltage DC power supply (15 kV), an injection pump used to control the flow rate of the polymer solution (1 mL/h), and a rotating drum collector (700 rpm).

syringe having an internal diameter of 15.7 mm was filled with the casting solution. A 19 gauge, 0.81 mm internal diameter metal needle was attached to the syringe. The syringe was placed in a syringe pump, and the casting solution was injected at a rate of 1 mL/h. The syringe was angled at approximately 10° horizontally to avoid falling drips at the capillary tip[20] and to ensure that the Taylor cone under the action of gravity is aligned with the center of the rotating collector. The positive terminal of the high-voltage DC power supply was connected to the metal needle, and the ground potential was given to the rotating collector. An aluminum foil was wrapped around the cylindrical collector for fiber collection. The potential difference between the needle and collector was set to 15 kV. The rotation of the collector was set to 700 rpm. The distance between the needle tip and the collector was set to 15 cm.[21] Electrospinning was performed under the ambient temperature of 22.2 °C. The casting solutions were

https://doi.org/10.1021/acsaenm.3c00245
ACS Appl. Eng. Mater. 2023, 1, 1924−1936

electrospun for 7 h and fibers were collected on the rotating collector. The fibers were dried for 1 day in open air.

2.5. Adsorption Procedure

The isotherm adsorption of MB by the ES fibers was studied using the initial dye concentration of 0.05 g/L in a pH range between 3 and 11. The pH of the solutions was adjusted using 0.1 M HCl and 0.1 M NaOH. Batch adsorption experiments were performed by adding 10 mg of each fiber (adsorbent) in 40 mL dye solution vials and shaking at 220 rpm for 24 h at room temperature, 23 °C.[22,23] After finishing the adsorption cycle, fibers were removed from the vials, and the concentration of the solution in the vials was measured using ultraviolet−visible spectroscopy at a wavelength of λ = 665 nm. A minimum of three replicates of each solution were prepared and tested, and an average value was reported. The adsorption percentage was determined using eq 1[24−26]

$$\% \text{ adsorption} = \frac{C_o - C_f}{C_o} \times 100 \quad (1)$$

where C_o is the initial concentration of MB in mg/L and C_f is the final concentration of MB in mg/L.

The adsorption capacity Q_e (mg/g) was calculated using eq 2[26,27]

$$Q_e = \frac{(C_o - C_e)V}{m} \quad (2)$$

where C_o (mg/L) and C_e (mg/L) are the initial and final concentrations, respectively, V is the volume of the solution (L), and m is the mass of the adsorbent (fibers) (g). The adsorption behavior was studied based on Langmuir and Freundlich adsorption isotherm models.

The Langmuir adsorption model is based on the assumption that monolayer (single layer) adsorption takes place on the surface of the adsorbate, and the thickness of the adsorbed layer is equal to one adsorbed molecule.[28] The equation describing the Langmuir model is[26]

$$q_e = \frac{Q_o K_L C_e}{1 + K_L C_e} \quad (3)$$

where q_e is the adsorption capacity at equilibrium (mg/g), C_e is the concentration of dye solution at equilibrium (mg/L), K_L is the Langmuir constant (L/g), which relates the affinity of the adsorbate toward the active sites, and Q_o is the maximum adsorption capacity (mg/g).

The Freundlich isotherm model assumes that there is multilayer adsorption.[29] The derivation of the Freundlich model is based on the assumption that the surface is heterogeneous and the distribution of adsorption heat over a surface is non-uniform.[28] The Freundlich model is quantified by[29]

$$\ln Q_e = \ln K_f + \frac{1}{n} \ln C_e \quad (4)$$

where $\frac{1}{n}$ (dimensionless) is the adsorption intensity of the adsorbent and K_f is the Freundlich constant ($L^{1/n} mg^{1-1/n} g^{-1}$) (adsorption capacity at unit concentration).

In addition to adsorption models, the adsorption kinetics for all the fabricated fibers were studied.

2.6. Regeneration and Reusability

The reusability of the fibers was investigated by performing five adsorption−desorption cycles. After each adsorption cycle, desorption was carried out by immersing the fibers in 0.01 M sodium hydroxide (NaOH) solution and shaking the solution at 220 rpm for 20−25 min, followed by washing the fibers several times with DI water to remove the excess dye and NaOH from the fibers. The fibers were then dried for use in the next adsorption cycle.[23] Each adsorption cycle was performed for 24 h. The dye removal percentage was calculated after each adsorption cycle using eq 1.

2.7. Characterization Techniques

Gel permeation chromatography (GPC) was performed using a Malvern Viscotek gel permeation chromatograph equipped with a refractive index detector, an automatic sampler, a pump, an injector, an inline degasser, a column oven (60 °C), and two in-series Malvern T6000M SEC columns. DMF was used as the mobile phase at a flow rate of 1 mL/min. The gas permeation chromatograph was calibrated against narrow molecular weight PS standards. A Brookfield viscometer (Cole-Parmer, Illinois, USA) was used to measure the viscosity of the casting solutions. The electrical conductivity of the casting solutions was measured using the Thermo Fisher conductivity meter (Waltham, Massachusetts, USA). The surface morphology of the ES fibers was determined using scanning electron microscopy (SEM, JEOL FE 7000, JEOL, Tokyo, Japan) with gold-coated samples. Energy-dispersive X-ray spectroscopy (EDX) (JEOL 7000, JEOL, Tokyo, Japan) was employed for elemental composition and map tracking of the ES fibers. Fourier transform infrared (FTIR) (PerkinElmer, Waltham, Massachusetts, USA) was used to determine the types of chemical bonds and functional groups in the fibers. The water contact angle (WCA) of the fibers was determined using the Bio Scientific Attention Theta Lite instrument (Avondale, Arizona, USA). The surface charge of the fibers was measured using Surpass 3 (Anton Paar, Houston, Texas, USA). The mechanical strength of the fibers was measured using the Test Resources Newton instrument (Shakopee, Minnesota, USA). The XRD analysis was conducted using a Bruker D2 Phaser powder X-ray diffractometer (Billerica, Massachusetts, USA) with a Cu tube as the X-ray source, a voltage of 30 kV, and a current of 10 mA.

3. RESULTS AND DISCUSSION

3.1. PVC Pipe, PVC Pool, PVC RG, and Casting Solution Characterization

The molecular weight of the polymer impacts the solution viscosity, which controls the properties of the fiber.[30] The number-average molecular weight (M_n), weight-average molecular weight (M_w), and polydispersity index (PDI) of all the samples were measured via GPC (Table 1), which was calibrated versus monodisperse PS standards.

Table 1. Number-Average Molecular Weight (M_n) (g/mol), Weight-Average Molecular Weight (M_w) (g/mol), and PDI of the PVC Pipe, PVC Pool Float, and RG PVC Using GPC

type of sample	M_n	M_w	PDI
RG PVC	90,664	175,451	1.9
PVC pipe	67,019	147,570	2.2
PVC pool float	101,760	180,656	1.7

The PVC from the pool float had a higher observed molecular weight than that of the PVC from the pipe, which is a consequence of the various grades of PVC used in the manufacturing of these materials (Table 1).

Since both the PVC pipe and PVC pool float are commercial products containing several additives, XRD analysis was done on an actual PVC pipe and PVC pool float to better understand the additives in their structure. The XRD pattern of the PVC pipe (Figure 2a) clearly showed the existence of calcium carbonate in the PVC pipe as the sharp (hkl) peak at a 2θ value of 29.4° corresponds to the (104) crystallographic plane of calcium carbonate.[31] The XRD pattern of the PVC pool float (Figure 2b) exhibited structures that confirm the existence of muscovite (mica) in the PVC pool float used as a filler to provide a silky/shiny luster. The sharp peaks at 2θ values of 9.03, 17.8, 26.7, 35.9, and 45.2° match exactly with the XRD peaks of muscovite reported in the literature.[32,33] The

https://doi.org/10.1021/acsaenm.3c00245
ACS Appl. Eng. Mater. 2023, 1, 1924−1936

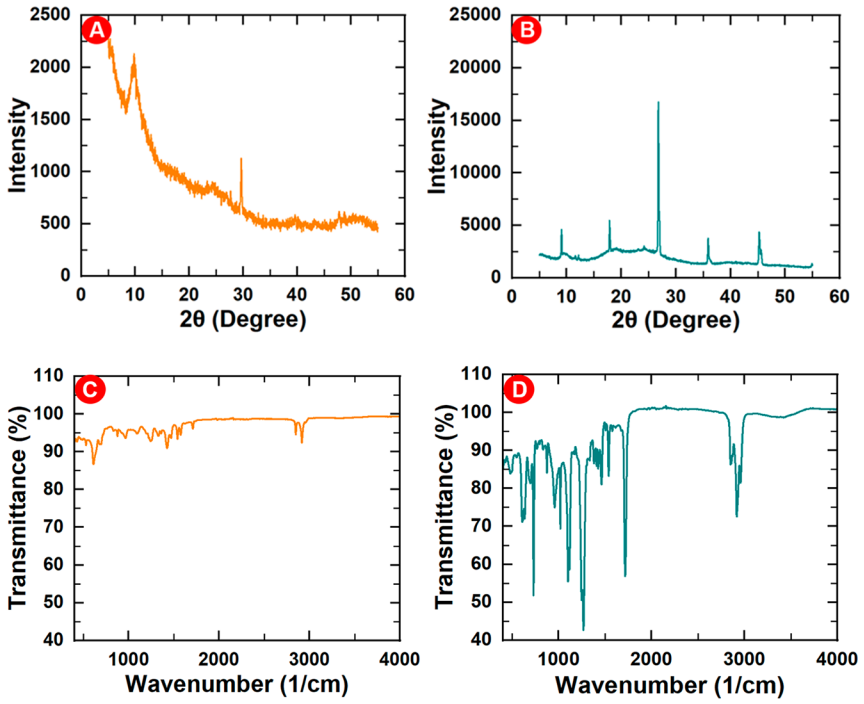

Figure 2. XRD pattern of a solid sample of the (a) PVC pipe and (b) pool float. FTIR of a solid sample of the (c) PVC pipe and (d) pool float. The PVC pipe samples were sanded before FTIR analysis.

FTIR spectra of a solid PVC pipe (Figure 2c) and a solid PVC pool float (Figure 2d) indicated the presence of additives such as adipate in the PVC pipe by the characteristic adipate peak at 1685 cm^{-1} and muscovite in the PVC pool by the peak at 1020 cm^{-1}, which represent the stretching and bending vibrational motions of Si−O bonds in the range of 950−1100 cm^{-1} and phthalates in the PVC pool float at 1730 cm^{-1} (C═O stretching vibration), the peak at 1575 cm^{-1} (C−C stretching vibration), the peak at 1599 cm^{-1} (C−C stretching vibration peaks of the benzene ring), and the peak at 745 cm^{-1} (ortho-substituted benzene stretching vibrations).[34,35] The FTIR of the solid PVC pipe (Figure 2c) and solid PVC pool float (Figure 2d) also showed the presence of calcium carbonate ($CaCO_3$) at 876 and 712 cm^{-1}.[36]

The viscosity at different shear rates for all six casting solutions is shown in Figure 3. All casting solutions show a Newtonian behavior, nearly constant viscosity at all shear rates.[37] The effects of two factors, including the polymer (PVC) concentration and additive ($CaCO_3$) concentrations, on the rheological behavior of casting solutions were studied. In one group of samples, the fixed amount (15 wt %) of RG PVC, PVC pipe, and PVC pool float was dissolved into the solvent, and their viscosity behaviors were compared. The RG PVC casting solution showed a higher viscosity compared to the other two casting solutions. The higher viscosity of RG PVC might be caused by the higher amount of PVC in the RG PVC casting solution since both the PVC pipe and PVC pool float had additives in their structure, which might have reduced their viscosity. In other words, portions of the added 15% (wt %) PVC pipe and PVC pool float were not pure PVC.

To clarify the effect of additives on viscosity, the viscosities of casting solutions with 3 and 8% $CaCO_3$ and 12 and 7% RG PVC were measured. The lower viscosities of 3 and 8% added $CaCO_3$ samples compared to pure RG PVC confirmed the reduction of viscosity due to the lower amount of polymer and

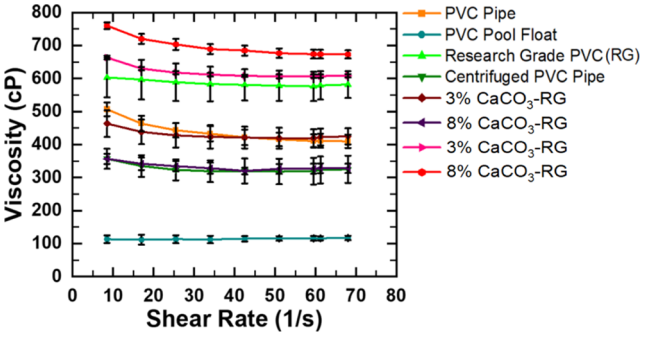

Figure 3. Viscosity (cP) vs shear rate (1/s) for the PVC pipe (orange), PVC pool float (blue), RG PVC (light green), centrifuged PVC pipe (dark green), 3% $CaCO_3$-RG (12%) (maroon), 8% $CaCO_3$-RG (7%) (purple), 3% $CaCO_3$-RG (15%) (pink), and 8% $CaCO_3$-RG (15%) (red) casting solutions. All casting solutions were prepared by dissolving an appropriate polymer concentration in a mixture of DMF and THF (v/v), 3:2, at 23 °C after stirring at 400 rpm for 19 h, followed by degassing for 4 h.

the existence of $CaCO_3$. In addition, a sample of the centrifuged PVC pipe casting solution in which most of the precipitated mass, including $CaCO_3$, was removed showed a lower viscosity compared to that of the PVC pipe, which confirms the role of polymer concentration in the viscosity of a casting solution. However, the addition of 3 and 8% (wt %) $CaCO_3$ while keeping a constant polymer content (15 wt %) increased the viscosity of samples since the presence of suspended insoluble $CaCO_3$ particles obstructed the flow of the casting solution during the applied shear rate and raised the flow resistance, i.e., the viscosity.

The electrical conductivity of the casting solutions is an important factor in electrospinning because it is strongly linked to the electrostatic force acting on the polymer casting solution.[38] The magnitude of this electrostatic force

https://doi.org/10.1021/acsaenm.3c00245
ACS Appl. Eng. Mater. 2023, 1, 1924−1936

determines the fiber diameters of the ES fibers.[39] In general, the higher conductivity of the casting solution, i.e., the more electrostatic force acting on the casting solution, results in the generation of more stretched fibers and smaller fiber diameters.[39] Figure 4 shows that all PVC casting solutions had very low conductivity. The highest conductivity was only 33.8 μS/cm for the PVC pipe. The reason for low conductivity lies in the PVC structure with strong carbon, hydrogen, and chlorine covalent bonds, which did not dissociate into ions after dissolving in the solvent. The conductivities of the PVC pipe and centrifuged PVC pipe casting solutions, followed by the PVC pool float, were significantly higher than those of the other solutions. Since the conductivity of $CaCO_3$-containing samples was in the same range as that of the RG PV, the presence of $CaCO_3$ in solutions was not the reason for the different conductivities. It is unclear at this time what causes the differences in conductivity. The adipate and phthalates are common additives to PVC products; however, since they exist in the ester form, they are not able to ionize and change the conductivity. Therefore, the change in conductivity might be due to the existence of trace quantities of other unknown additives that need to be investigated.

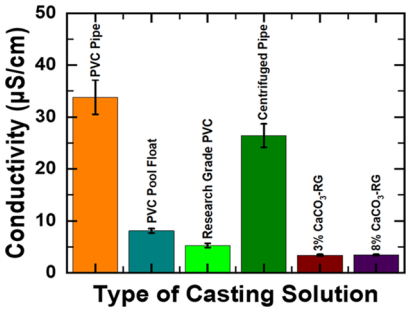

Figure 4. Conductivities of the PVC pipe, PVC pool float, RG PVC, centrifuged PVC pipe, 3% $CaCO_3$-RG, and 8% $CaCO_3$-RG casting solutions were measured at 23 °C after stirring at 400 rpm for 19 h, followed by degassing for 4 h.

3.2. Fiber Characterization

The chemical bonds and functional groups present in the fibers were investigated by FTIR spectroscopy (Figure 5). The FTIR spectra of all six fibers were recorded at room temperature in the 450−4000 cm^{-1} range. Most of the signals in the FTIR spectra of PVC pipe fibers and PVC pool fibers matched the signals in the FTIR spectra of the RG PVC fibers; however, there were a few new peaks. The matching signals in all three spectra include the peaks at 618, 636, and 689 cm^{-1} corresponding to C−Cl stretching, the peak at 960 cm^{-1} indicating rocking CH_2, the peak at 1097 cm^{-1}representing a stretching C−C bond, the two peaks at 1252 and 1330 cm^{-1} are for deformation of the C−H bond of CHCl, the peak at 1428 cm^{-1} represents deformation (wagg) of CH_2, the peak at 2912 cm^{-1} corresponds to stretching of the C−H bond of CH_2, and the peak at 2973 cm^{-1} indicates stretching of the C−H bond of CHCl. The signals at 712 and 875 cm^{-1} in the PVC pipe spectra correspond to calcium carbonate ($CaCO_3$) and the signal at 728 cm^{-1} indicates calcium carbonate in the PVC pool float.

The FTIR spectra of centrifuged PVC pipe fibers were very similar to those of the RG PVC fibers, which showed that most of the additives of the PVC pipe were separated into the centrifuged sediment. In the FTIR of centrifuged PVC pipe fibers, the peak from 600 to 690 cm^{-1} represents the C−Cl gauche bond. The peak at 844 cm^{-1} corresponds to C−Cl stretching. The peak at 961 cm^{-1} represents *Trans*-CH wagging. The peaks from 1240 to 1257 cm^{-1} indicate CH rocking. The CH_2 deformation peak appears at 1339 cm^{-1}. The peaks from 2890 to 2958 cm^{-1} are for CH stretching.[40] The FTIR spectra of the centrifuged sediment, solid content at the bottom of the vial after the PVC pipe casting solution was centrifuged, clearly showed the existence of calcium carbonate ($CaCO_3$) (Figure 5f). The peak at 870 cm^{-1} indicates the out-of-plane bending absorption of carbonate ions. The peak at

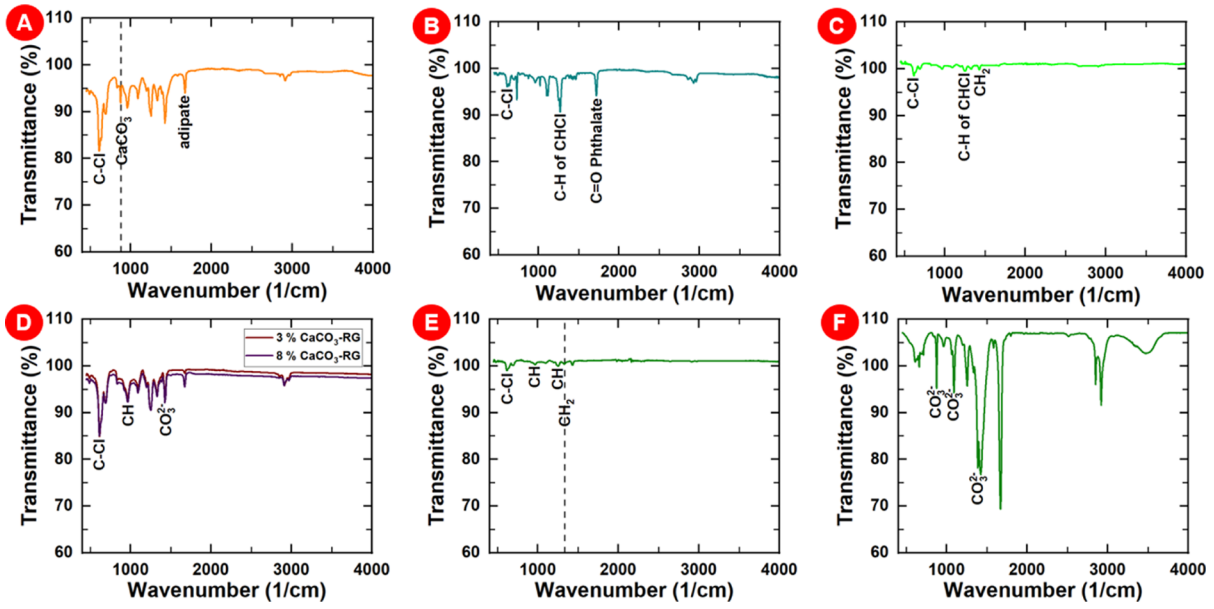

Figure 5. FTIR spectra of (a) PVC pipe fibers, (b) PVC pool float fibers, (c) RG PVC fibers, (d) 3 and 8% $CaCO_3$-RG fibers, (e) centrifuged PVC pipe fibers, and (f) white solid ($CaCO_3$) deposited at the bottom of the vial after centrifuging the PVC pipe casting solution. See Figure S1 for the magnified plots.

https://doi.org/10.1021/acsaenm.3c00245
ACS Appl. Eng. Mater. 2023, 1, 1924−1936

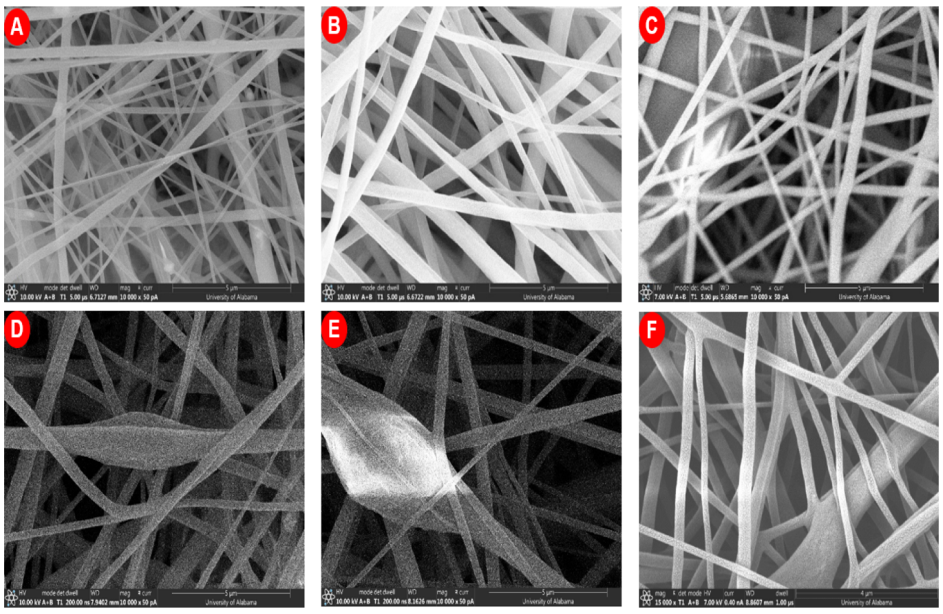

Figure 6. SEM image of (a) PVC pipe fibers, (b) RG PVC fibers, (c) PVC pool float fibers, (d) 8% $CaCO_3$-RG fibers, (e) 3% $CaCO_3$-RG fibers, and (f) centrifuged PVC pipe fibers. All fibers were made at the THF/DMF (2:3) volume ratio, 15 wt % total casting solution concentration, 1 mL/h solution injection rate, a 15 kV applied voltage, a 15 cm tip to collector distance, and a 700 rpm collector speed. Prior to SEM, the samples were gold sputtered at a 6 mA current for 90 s.

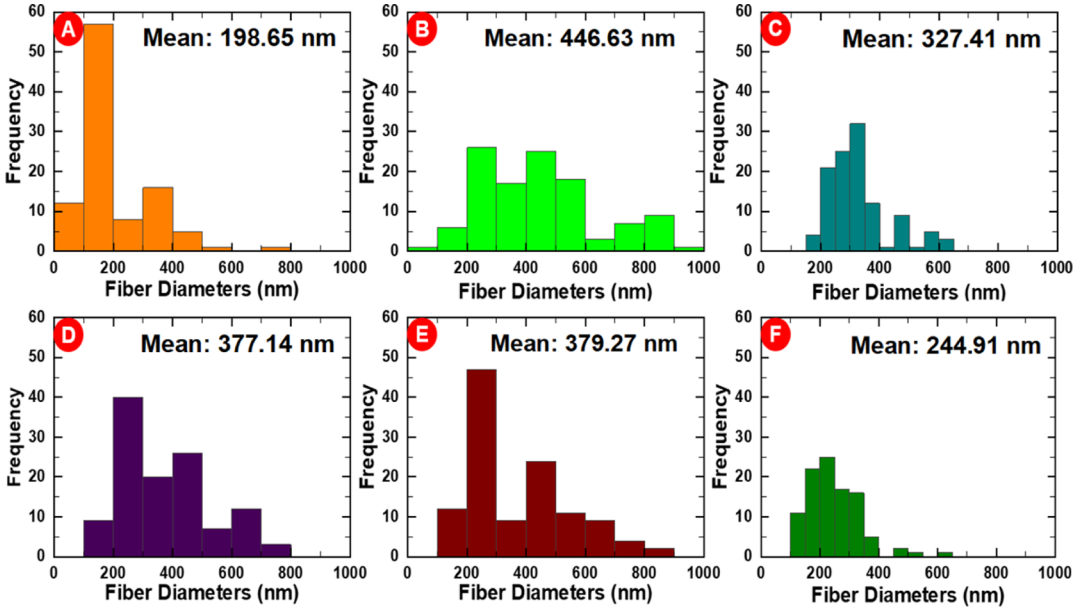

Figure 7. Fiber diameter (nm) distribution of (a) PVC pipe fibers, (b) RG PVC fibers, (c) PVC pool float fibers, (d) 8% $CaCO_3$-RG fibers, (e) 3% $CaCO_3$-RG fibers, and (f) centrifuged PVC pipe fibers measured at 100 different points using ImageJ software.

1080 cm^{-1} represents the symmetric stretch of the carbonate ion.[36] The FTIR spectra of 3 and 8% $CaCO_3$-RG showed peaks that confirmed the presence of both $CaCO_3$ and PVC. The peaks from 600 to 650 cm^{-1} represent the C−Cl gauche bond in PVC.[41] The peak at 700 cm^{-1} represents the in-plane bending of the carbonate ion. The peak at 961 cm^{-1} represents *Trans*-CH wagging in PVC. The peak at 1080 cm^{-1} is for the symmetric stretch of the carbonate ion. The PVC peak between 1240 and 1257 cm^{-1} represents CH rocking while the peak at 1339 cm^{-1} represents CH_2 deformation. The peak at 1420 cm^{-1} is for the asymmetric stretch of the carbonate ion. The PVC peak from 2890 to 2958 cm^{-1} indicates C−H stretching.[36,40] The FTIR spectra of the PVC pool float showed the presence of phthalate. The peak at 1730 cm^{-1} corresponds to C═O stretching vibration. The peaks at 1575 and 1599 cm^{-1} are for the C−C stretching vibration peaks of the benzene ring. The band at 745 cm^{-1} represents ortho-substituted benzene stretching vibrations.[34] As it was observed in the FTIR spectrum of a solid sample of the PVC float, the stretching and bending vibrational motions of Si−O in the range of 950−1100 cm^{-1} imply the presence of muscovite. The peaks between 500 and 1300 cm^{-1} correspond to vibrations in the aluminosilicate layers in muscovite.[35] Furthermore, the presence of adipate in the PVC pipe and centrifuged sediment

https://doi.org/10.1021/acsaenm.3c00245
ACS Appl. Eng. Mater. 2023, 1, 1924−1936

(white solid) is represented by the characteristic adipate peak at 1685 cm^{-1}, which represents the stretching vibration of the −COOH groups.[42]

SEM was employed to analyze the morphology of the six ES nanofibers (Figure 6). All fabricated fibers showed the typical randomly organized nanofibrous structure of ES fibers although they differed based on fiber diameter and bead formation. Different fiber properties for each sample were observed from the SEM images. The casting solution conductivity and viscosity are the two main factors controlling the fiber morphology.[43] In general, higher conductivity of a casting solution and lower viscosity of the casting solution result in more stretching of the fibers during electrospinning, which generate thinner fibers.[39] The fiber diameters followed the order of PVC pipe < centrifuged PVC pipe < PVC pool float < 8% $CaCO_3$-RG ≈ 3% $CaCO_3$-RG < RG PVC (Figure 7). As discussed earlier (Figure 4), the PVC pipe and centrifuged PVC pipe casting solutions had higher conductivities than those of other casting solutions. Therefore, their ES fibers were generated in a more stretched form with thinner fiber diameters. The PVC pool float also had a higher conductivity than 8 and 3% $CaCO_3$-RG and RG PVC; hence it produced fibers of lower diameters. 8 and 3% $CaCO_3$-RG casting solutions had almost the same electrical conductivities, resulting in nearly the same mean fiber diameters. As mentioned earlier, the viscosity of the casting solution is the other factor affecting the fiber diameter. A higher viscosity provides more entanglement between the polymer chains and, therefore, enhanced resistance to stretching during the electrospinning process, which may result in a thicker fiber diameter. In this regard, the thicker fibers of RG PVC can be attributed to its high viscosity among all the casting solutions (Figure 3).[44,45] It can also be observed from SEM images and the fiber diameter distribution plots (Figures 6 and 7) that the addition of $CaCO_3$ reduced the fiber diameter compared to the RG PVC. PVC consists of polar molecules via dipole−dipole interaction between the chlorine atom of one molecule to a hydrogen atom in another molecule.[14] One possible explanation for the reduced fiber diameter of $CaCO_3$-containing samples could be the enhanced extension of PVC fibers due to the repulsion of positively charged $CaCO_3$ under the positive charge field applied on the needle during electrospinning that causes the PVC chains to move further apart from one another. The SEM images (Figure 6) show that the alignment orientation of centrifuged PVC pipe nanofibers is least random, i.e., the nanofibers are more aligned compared to nanofibers in other fibers.

The alignment of nanofibers is affected by the electrical conductivity and viscosity of the solution. The possible reason for more aligned nanofibers with the centrifuged PVC pipe casting solution compared to other fibers is that it has a higher electrical conductivity and lower viscosity compared to the other solutions. Higher electrical conductivity leads to larger electrostatic force and faster movement of fibers to the collector, thereby reducing chain defection (whipping instabilities) and producing aligned/oriented nanofibers. Lower viscosities caused fibers to experience less gravitational force and hence less deflection in the vertical direction, leading to the formation of aligned/oriented nanofibers. The low molecular weight/concentration/viscosity and low charge density are the two main causes of bead formation in electrospinning.[46] Fluids with a low relaxation time or shear viscosity tend to form beads. The stretching force to elongate the solution is represented by the charge density on the electrospinning jet. Inadequate charge density causes insufficient elongation viscosity to counteract Rayleigh instability, resulting in the formation of beads.[46,47] Also, additives might affect the bead formation based on their solubility in the solvent.[48−50]

In general, a soluble additive such as a salt leads to higher conductivity of the casting solution and an increased net charge density on the jet, which strengthen the elongation force and decrease the bead formation.[48] The presence of insoluble additives (e.g., $CaCO_3$) leads to additive particles blooming along the fiber due to a higher degree of the local particle agglomeration during the electrospinning process, which can lead to increased bead formation. The local particle agglomeration might be caused by a heterogeneous distribution of the particles in casting solutions during electrospinning.[49] Figure 8 shows that PVC pipe fibers possessed a higher number of beads than the RG fibers. The viscosity of the PVC pipe was lower than that of RG PVC (Figure 3), while the conductivity of the PVC pipe was higher than that of RG (Figure 4). Thus, it can be concluded that the effect of viscosity was more dominant than conductivity on the bead formation. It should be noted that, in general, the conductivity of all samples was relatively low (3−32 μS/cm), which confirms the lower conductivity effect on bead formation. Also, the higher number of beads in the PVC pipe might be due to the aggregation of $CaCO_3$ during electrospinning, which resulted as beads in the fibers. The $CaCO_3$ aggregation was confirmed by detecting clusters of $CaCO_3$ with a higher number of $CaCO_3$ particles inside the beads compared to the rest of the fibers (Figure 9).[49] In addition, the higher number of beads in 8% $CaCO_3$-RG and 3% $CaCO_3$-RG fibers compared to the RG PVC confirmed the effect of $CaCO_3$ and viscosity on the bead formation. The centrifuged PVC pipe fibers showed a lower number of beads compared to all the $CaCO_3$-containing samples, which confirmed that the removal of $CaCO_3$ by centrifugation resulted in less bead formation. Also, the lower number of beads on centrifuged PVC pipe fibers (mats) compared to the non-centrifuged PVC pipe should be due to the removal of $CaCO_3$ since the viscosity and conductivity of the PVC centrifuged casting solution were lower than that of the pipe (Figures 3 and 4).

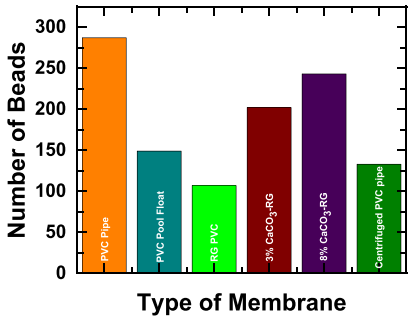

Figure 8. Number of beads in the PVC pipe, PVC pool float, RG PVC, 3% $CaCO_3$-RG, 8% $CaCO_3$-RG, and centrifuged PVC pipe fibers. The reported data are the result of analyzing at least three different samples of each fiber.

Surface hydrophilicity is an important factor in the separation or adsorption process. The chemical composition and surface topography (surface roughness) are the key points controlling the hydrophobicity of ES fibers.[51] The hydro-

https://doi.org/10.1021/acsaenm.3c00245
ACS Appl. Eng. Mater. 2023, 1, 1924−1936

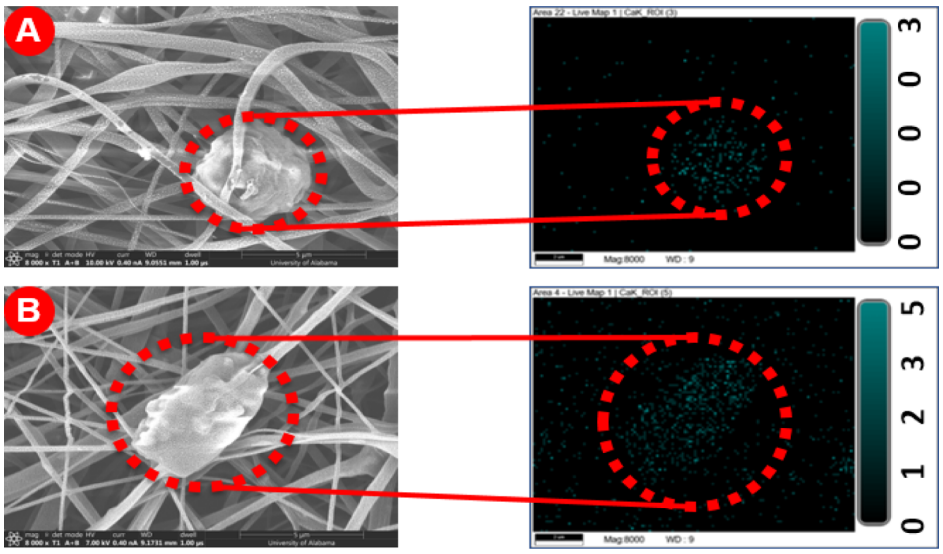

Figure 9. EDX mapping of (a) 8% $CaCO_3$-RG fibers and (b) PVC pipe fibers confirming calcium carbonate ($CaCO_3$) clusters inside the beads.

philicity degree of the fibers was determined using the WCA. A surface is hydrophobic when the contact angle is greater than 90° and hydrophilic when it is less than 90°.[52,53]

Figure 10 shows the mean WCA measured at a minimum of 15 different points on each of the six ES fibers. The

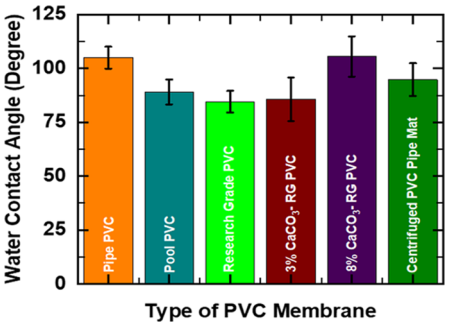

Figure 10. WCA for PVC pipe fibers, PVC pool float fibers, RG PVC fibers, 3% $CaCO_3$-RG fibers, 8% $CaCO_3$-RG fibers, and centrifuged PVC pipe fibers.

interactions of PVC with water molecules are due to strong dipole−dipole interactions between the partial negative chlorine atom of PVC and the partially positive hydrogen atom of a water molecule. The presence of other hydrophobic additives such as adipate and phthalate (Figure 5a,b) (Figure S2a,c) in the PVC pipe and pool float could be the reason for the higher hydrophobicity of these fibers.[54] Another factor that physically affects the hydrophobic behavior of the ES fibers is fiber diameter. In general, larger fiber diameters contribute to lower WCA.[55] The larger the fiber diameter (cylinders with a larger radius), the more the surface area the fiber has, which provides an extended surface for water, leading to a decrease in contact angle and hence hydrophilic behavior (Figure S3a,b).[55] Therefore, the higher hydrophobicity of the PVC pipe and PVC pool float compared to RG PVC might also be due to the smaller diameter of fibers in the PVC pipe and PVC pool float (Figure 7). Furthermore, beads on the fibers also contribute to a higher WCA.[55,56] Beads can be assumed to act as spheres with a much smaller surface area than fibers (with cylindrical geometry) on which a water drop can spread. Hence, beads increase the contact angle and make the surface more hydrophobic (Figure S3c).[55] Also, because the beads possess agglomerated $CaCO_3$ (Figure 9), the surface of the beads possessed a hills and valleys structure or protuberant characteristics, contributing to the increased hydrophobicity of the PVC pipe. The fibers fabricated using the centrifuged PVC pipe casting solution also showed higher hydrophobicity compared to RG PVC but lower than the PVC pipe fibers. This might indicate the presence of plasticizers such as adipates or phthalates (which are hydrophobic in nature due to their long hydrocarbon chains and the aromatic benzene ring, respectively) in the supernatant of the centrifuged solution, which did not sediment by centrifugation.[54]

The surface charges of all six fibers were measured in a range of pH (3−11) as shown in Figure 11. All fibers showed a

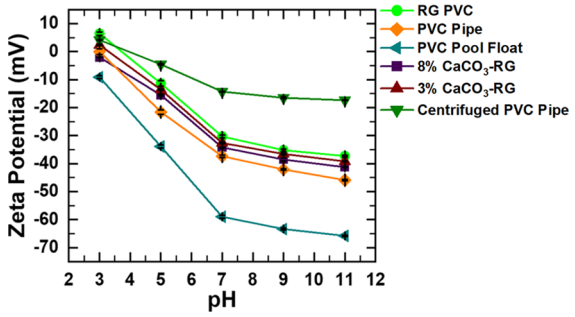

Figure 11. Zeta potential of PVC pipe fibers, PVC pool float fibers, RG PVC fibers, 3% $CaCO_3$-RG fibers, 8% $CaCO_3$-RG fibers, and centrifuged PVC pipe fibers in acidic (pH 3−5), neutral (pH 7), and basic (pH 9−11) pH.

negative surface charge. It was reported by other groups that this behavior could be due to defects in the PVC structure or additives.[57,58] The reason for the higher negative surface charge of the PVC pipe and pool float compared to RG PVC might be the presence of additives, including calcium carbonate ($CaCO_3$). Almost all the ES fibers showed a similar surface charge except the fibers fabricated by the centrifuged PVC pipe casting solution and pool float. Centrifuged PVC pipe fibers showed the least negative surface charge among the

https://doi.org/10.1021/acsaenm.3c00245
ACS Appl. Eng. Mater. 2023, 1, 1924−1936

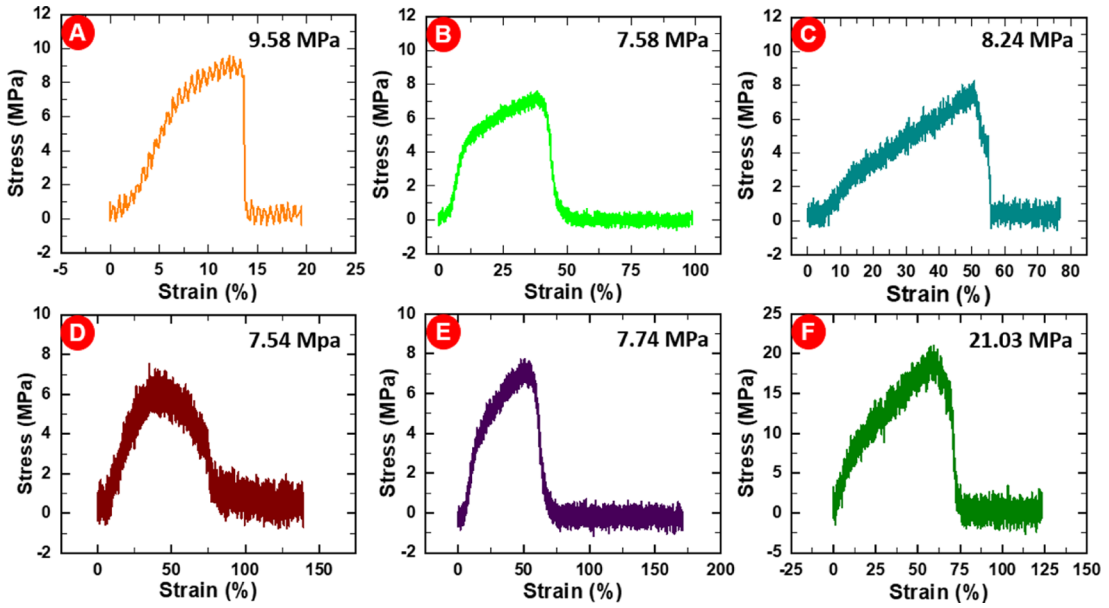

Figure 12. Stress−strain curves for (a) PVC pipe fibers, (b) RG PVC fibers, (c) PVC pool float fibers, (d) 3% $CaCO_3$-RG fibers, (e) 8% $CaCO_3$-RG fibers, and (f) centrifuged PVC pipe fibers.

ES fibers. However, the exact roles of various additive variations in zeta potential are unclear.

The ES fibers were tested for mechanical strength, and the stress−strain plots of all six fibers are shown in Figure 12.

The maximum bearable stress of centrifuged PVC pipe fibers (mat) is much higher than the maximum bearable stress of other fibers (Figure 12). The reason for this behavior lies in the alignment orientation of ES fibers. A major factor that influences the mechanical properties of fibers is the anisotropy of fibers.[21] Randomly distributed fibers lead to a lower mechanical strength compared to oriented nanofibers.[21]

As was discussed based on the SEM images (Figure 6), the centrifuged PVC pipe nanofibers possessed a more aligned fiber structure (due to the higher electrical conductivity and lower viscosity) compared to fibers in other mats, resulting in the high bearable stress of 21.03 MPa. It is also observed that the PVC pipe fibers showed the second-highest strain at break among the samples. One reason for the higher mechanical strength of the PVC pool and PVC pipe might be the existence of additives in these materials. The 3 and 8% $CaCO_3$-RG samples did not show a significant difference compared to the RG PVC, which indicates that $CaCO_3$ did not have any effect on the strength of fibers. One possible justification for the PVC pipe fibers might be their small fiber diameter (198.65 nm) among the fibers. Generally, a decrease in nanofiber diameter resulted in enhanced tensile strength since at a lower diameter of ES nanofibers, the molecular orientation and degree of crystallinity of the nanofibers are increased, leading to improved mechanical strength and stiffness.[21,59]

3.3. Fiber Performance: Adsorption Model and Kinetics

The adsorption performances of all the fabricated fibers were evaluated using MB as a common contaminant in water.[60] The removal efficiency of all six fibers was tested by calculating the percentage of MB adsorbed by the fibers at different pH values (Figure 13).

The adsorption of MB on the fibers was confirmed through EDX mapping of the fibers after adsorption. EDX showed the

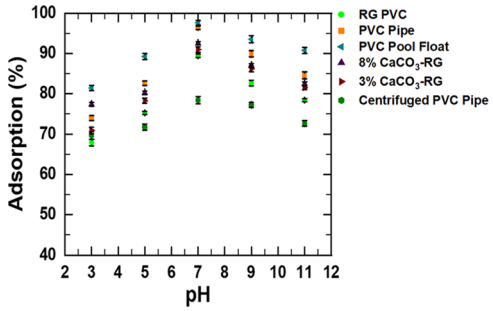

Figure 13. Adsorption performance (%) of ES fibers for the removal of MB from water. Static adsorption was performed using an initial MB concentration of 50 ppm (0.05 g/L), 10 mg of each fiber, a shaking speed of 220 rpm for 24 h, and a room temperature of 23 °C.

presence of nitrogen and sulfur atoms of MB in addition to the carbon and chlorine atoms of the PVC fibers (Figure 14).

Figure 13 shows that throughout the pH range from pH 3 to 11, the MB removal percentage by fibers follows the order of PVC pool float > PVC pipe > 8% $CaCO_3$-RG > 3% $CaCO_3$-RG > RG PVC > centrifuged PVC pipe mat. The reason for this trend is the electrostatic adsorption mechanism between the fibers and MB where at all pH values, the surface charge of the fibers followed the order of most negative to least negative: PVC pool float > PVC pipe > 8% $CaCO_3$-RG > 3% $CaCO_3$-RG > RG PVC > centrifuged PVC pipe mat (Figure 11). MB, a cationic dye with a positive zeta potential at all pH values, was electrostatically attracted to the negative surface of the fibers.[22,23,61] The higher the negative surface charge of the fibers, the more the electrostatic interaction between the fibers and cationic MB; hence, the greater the adsorption of MB by the fibers. The highest adsorption takes place at pH 7.

The reason for the highest adsorption at pH = 7 is the different interactions between fibers and MB at acidic and basic pH. Due to the abundance of H^+ in acidic pH, H^+ competes with MB in interaction with fibers (adsorption) and therefore reduces the number of active sites for the adsorption of MB.[62,63] Moreover, in acidic pH, the surface charge of the

https://doi.org/10.1021/acsaenm.3c00245
ACS Appl. Eng. Mater. 2023, 1, 1924−1936

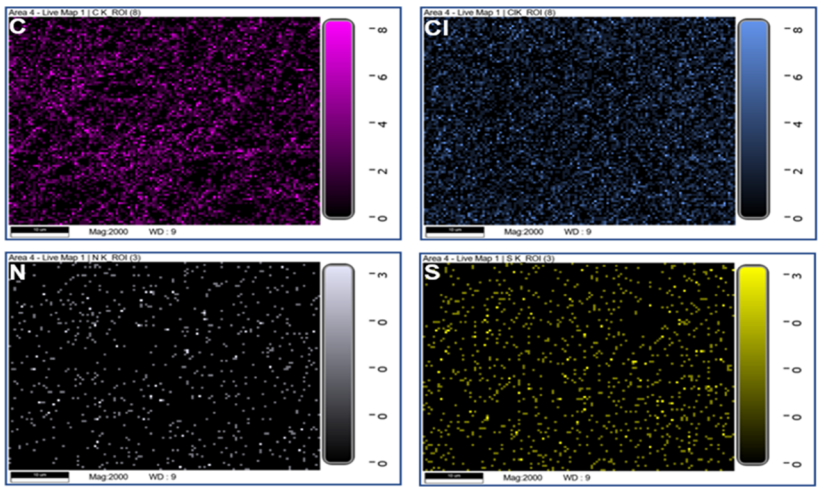

Figure 14. EDX mapping of fibers after adsorption of MB shows the presence of nitrogen and sulfur on the fibers, hence confirming the adsorption of MB. Static adsorption was performed using an initial MB concentration of 50 ppm (0.05 g/L), 10 mg of each fiber, a shaking speed of 220 rpm for 24 h, and a room temperature of 23 °C.

Table 2. Comparison between the Performance of Upcycled PVC Fibers (PVC Pipe and PVC Pool Float) with Other ES Fibers in Dye Removal from Water

type of fibers	adsorption time (min)	initial concentration of MB (ppm)	MB removal (%) or adsorption capacity (mg/g)	references
cellulose acetate nanofibrous membranes modified by polydopamine	1440	50	93.21%	61
PAN/β-CD nanofiber membrane	600	300	108.66 mg/g	65
β-cyclodextrin-based ES nanofiber membranes	360	40	826.45 mg/g	66
p(*N*-isopropyl acrylamide-*co*-β-cyclodextrin) (PNCD) and *p*(*N*-isopropyl acrylamide-*co*-methacrylicacid) (PNMA) polydopamine microsphere (PDA-MP) composite fibers (PNCD-PNMA/PDAs-MPs)	700	50	1722.1 mg/g	67
polyvinyl butyral/bentonite	420	100	86%	68
polylactic acid (PLLA) and polyacrylonitrile (PAN) coated with chloride-doped polyaniline (PANI)	(PLLA/PANI) 1440	300	135 mg/g	62
	(PAN/PANI) 1440	300	140 mg/g	
gelatin/alginate composite nanofiber membranes	240	500	1937 mg/g	69
polyether sulfone and hydroxypropyl cellulose (PES/HPC)	1440	400	259.74 mg/g	70
PVC pipe	**1440**	**50**	96.39% **(192.78 mg/g)**	**this work**
PVC pool float	**1440**	**50**	97.64% **(195.28 mg/g)**	**this work**

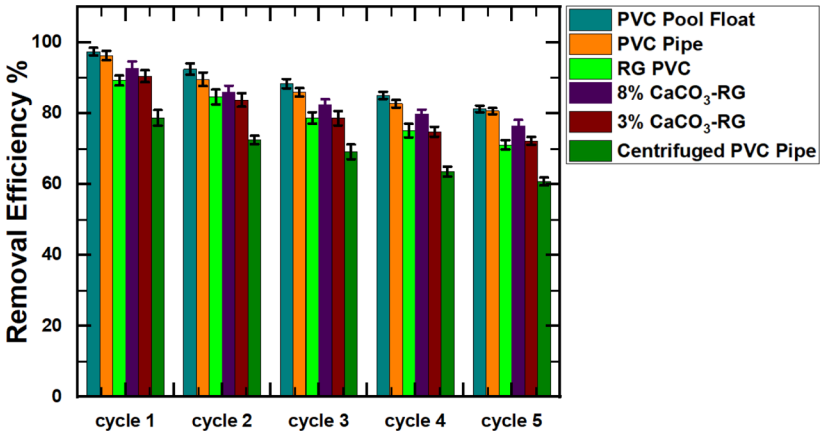

Figure 15. Regeneration cycles (adsorption−desorption cycles) of all fibers. All fibers were regenerated using 0.01 M NaOH and each adsorption cycle was performed for 24 h.

fibers was less than pH = 7 (Figure 11), leading to weaker electrostatic interactions between the dye and fibers. Furthermore, in acidic pH, there would be hydrogen bonding between the lone pair of highly electronegative N atoms in MB

https://doi.org/10.1021/acsaenm.3c00245
ACS Appl. Eng. Mater. 2023, 1, 1924−1936

and positive hydrogen ions. Hydrogen bonding is stronger than the electrostatic attraction between MB and the negative surface of the fibers, leading to decreased adsorption of MB by the fibers.[64] In basic pH, there are more OH^- ions, and hence MB can have electrostatic interactions with these OH^- ions, which might reduce the number of MB molecules electrostatically interacting with the negative fibers.[63] In addition, there might be hydrogen bonding between MB and OH^- ions, which results in a lower number of available MB to interact with the surface of the fibers, which decreases the adsorption of MB by fibers in basic pH.[64] The performance of both upcycled PVC fibers (PVC pipe and PVC pool float) was compared with that of other ES fibers fabricated by other polymers, as shown in Table 2. It is evident that the adsorption of MB by PVC pipe and PVC pool float fibers is in the range or even higher than other reported data, showing the feasibility of the upcycled PVC fibers in water and wastewater treatment. The results showed that the adsorption behavior best fitted the Freundlich adsorption model, which indicates the multilayer adsorption of MB onto the surface of the nanofiber and a heterogeneous surface of the nanofiber mats (adsorbent).[26] A kinetic study indicated that the adsorption mostly follows pseudo-1st-order kinetics, which implies physisorption (electrostatic interaction) mechanism as discussed earlier. The kinetic study revealed the adsorption equilibrium of 5 h for the PVC pipe and PVC pool float fibers, 6 h for RG-PVC, 3% $CaCO_3$-RG and 8% $CaCO_3$-RG fibers, and 7 h for centrifuged PVC pipe fibers.

3.4. Regeneration and Reusability

The results of 5 cycles of adsorption−desorption are presented in Figure 15. All the fibers showed a decrease in dye removal during the regeneration process. The waste PVCs (PVC pool float and PVC pipe) showed the highest adsorption even after 5 cycles, with a removal efficiency of more than 80%, while the removal efficiency of RG PVC after 5 cycles was around 71%. The results show that both upcycled PVC pipe and pool showed acceptable re-generality, with only around 16.3 and 16.6% reduction of adsorption, respectively.

4. CONCLUSIONS

In this study, waste PVC materials such as the PVC pipe and PVC pool float were successfully upcycled to fibers by the electrospinning process. The upcycling process of the waste PVC pipe and waste pool float to fibers was evaluated based on the fiber fabrication process and fiber performance in water treatment and was compared to that of the RG PVC. In terms of fiber fabrication, the viscosity and conductivity of casting solutions impacted the fiber morphology, fiber diameter, and mechanical stability of ES fibers. The waste PVC pipe casting solutions showed higher electrical conductivity and lower viscosity than the RG casting solution, resulting in a thinner fiber diameter. In addition, the effect of additives such as $CaCO_3$ in the waste PVC pipe and PVC pool float on the upcycled fibers was studied. It was found that the presence of $CaCO_3$ in the waste PVC pipe resulted in higher hydrophobicity, lower fiber diameter, and higher mechanical strength compared to RG PVC. In addition, the presence of $CaCO_3$ in the waste PVC pipe increased the hydrophobicity and mechanical strength of the ES fibers compared to ES fibers fabricated from RG PVC. Both waste PVC pipe and pool float fibers showed higher negative surface charge compared to RG PVC fibers. In terms of water treatment performance as adsorptive fibers, both upcycled PVC pipe and PVC pool float fibers showed enhanced removal efficiencies of 97.64 and 96.39%, respectively, compared to 89.41% removal by RG PVC fibers. Furthermore, the reusability of the fabricated fibers was investigated by performing five adsorption−desorption cycles. The results indicated that the upcycled PVC pool PVC pipe showed an acceptable removal efficiency of over 80%. This study clearly shows the potential of upcycling PVC waste materials from landfill into fibers for enhanced water treatment as a promising solution to the current plastic pollution.

■ ASSOCIATED CONTENT

Supporting Information

The Supporting Information is available free of charge at https://pubs.acs.org/doi/10.1021/acsaenm.3c00245.

Information on molecular weight measurements; FTIR spectra and EDX analysis of different fibers; effect of ES fiber diameter and beads on the WCA of the fibers; Langmuir and Freundlich adsorption isotherms; adsorption kinetics; FTIR peaks, low-resolution SEM images of the fibers; and optical images of the contact angles of the nanofiber mats with water droplets during WCA measurements (PDF)

■ AUTHOR INFORMATION

Corresponding Author

Milad Rabbani Esfahani − *Department of Chemical and Biological Engineering, University of Alabama, Tuscaloosa, Alabama 35487, United States;* orcid.org/0000-0001-6530-4310; Phone: 205-348-8836; Email: mesfahani@eng.ua.edu

Authors

Atta Ur Razzaq − *Department of Chemical and Biological Engineering, University of Alabama, Tuscaloosa, Alabama 35487, United States*

D. J. McEachern − *Department of Chemistry and Biochemistry, University of Alabama, Tuscaloosa, Alabama 35487, United States*

Paul A. Rupar − *Department of Chemistry and Biochemistry, University of Alabama, Tuscaloosa, Alabama 35487, United States;* orcid.org/0000-0002-9532-116X

Phoebe R. Willis − *Department of Chemistry and Biochemistry, University of Alabama, Tuscaloosa, Alabama 35487, United States*

S. Nima Mahmoodi − *Department of Mechanical Engineering, University of Alabama, Tuscaloosa, Alabama 35487, United States*

Complete contact information is available at: https://pubs.acs.org/10.1021/acsaenm.3c00245

Notes

The authors declare no competing financial interest.

■ ACKNOWLEDGMENTS

The authors thank the National Science Foundation (NSF) for the financial support under Award no. 2029387. Prof. Jason E. Bara and Ali Al Alshaikh are acknowledged for their insightful discussion. The authors gratefully thank the Department of Chemical and Biological Engineering at the University of Alabama and the Alabama Water Institute at the University of Alabama for instrumental support.

REFERENCES

(1) Saleem, J.; Adil Riaz, M.; Gordon, M. Oil sorbents from plastic wastes and polymers: A review. *J. Hazard Mater.* **2018**, *341*, 424−437.
(2) Li, X.; Peng, Y.; Deng, Y.; Ye, F.; Zhang, C.; Hu, X.; Liu, Y.; Zhang, D. Recycling and Reutilizing Polymer Waste via Electrospun Micro/Nanofibers: A Review. *Nanomaterials* **2022**, *12*, 1663−1680.
(3) Pan, D.; Su, F.; Liu, C.; Guo, Z. Research progress for plastic waste management and manufacture of value-added products. *Adv. Compos. Hybrid Mater.* **2020**, *3*, 443−461.
(4) Al-Salem, S. M.; Lettieri, P.; Baeyens, J. Recycling and recovery routes of plastic solid waste (PSW): a review. *Waste Manag.* **2009**, *29*, 2625−2643.
(5) Briassoulis, D.; Hiskakis, M.; Babou, E. Technical specifications for mechanical recycling of agricultural plastic waste. *Waste Manag.* **2013**, *33*, 1516−1530.
(6) Bujak, J. W. Thermal utilization (treatment) of plastic waste. *Energy* **2015**, *90*, 1468−1477.
(7) Hopewell, J.; Dvorak, R.; Kosior, E. Plastics recycling: challenges and opportunities. *Philos. Trans. R. Soc., B* **2009**, *364*, 2115−2126.
(8) Hou, Q.; Zhen, M.; Qian, H.; Nie, Y.; Bai, X.; Xia, T.; Laiq Ur Rehman, M.; Li, Q.; Ju, M. Upcycling and catalytic degradation of plastic wastes. *Cell Rep. Phys. Sci.* **2021**, *2*, 100514−100544.
(9) Janajreh, I.; Alshrah, M.; Zamzam, S. Mechanical recycling of PVC plastic waste streams from cable industry: A case study. *Sustain. Cities Soc.* **2015**, *18*, 13−20.
(10) Soltan, A. M.; Taman, Z.; El-Kaliouby, B. Recycling of Ornamental Stones Hazardous Wastes. *Nat. Resour.* **2011**, *02*, 244−249.
(11) Luciani, V.; Bonifazi, G.; Rem, P.; Serranti, S. Upgrading of PVC rich wastes by magnetic density separation and hyperspectral imaging quality control. *Waste Manag.* **2015**, *45*, 118−125.
(12) Zulfi, A.; Rezeki, Y. A.; Edikresnha, D.; Munir, M. M.; Khairurrijal, K. Synthesis of Fibers and Particles from Polyvinyl Chloride (PVC) Waste Using Electrospinning. *IOP Conf. Ser.: Mater. Sci. Eng.* **2018**, *367*, 012014.
(13) Wang, Z.; Kang, S. B.; Yun, H. J.; Won, S. W. Efficient removal of arsenate from water using electrospun polyethylenimine/polyvinyl chloride nanofiber sheets. *React. Funct. Polym.* **2023**, *184*, 105514.
(14) Yuan, J.; Cheng, B. A Strategy for Nonmigrating Highly Plasticized PVC. *Sci. Rep.* **2017**, *7*, 9277.
(15) Geyer, R.; Jambeck, J. R.; Law, K. L. Production, use, and fate of all plastics ever made. *Sci. Adv.* **2017**, *3*, e1700782−e1700787.
(16) Tang, Y.; Cai, Z.; Sun, X.; Chong, C.; Yan, X.; Li, M.; Xu, J. Electrospun Nanofiber-Based Membranes for Water Treatment. *Polymers* **2022**, *14*, 2004.
(17) Yekrang, J.; Mohseni, L.; Etemadi, H. Water Treatment Using PVC/TPU/PC Electrospun Nanofiber Membranes. *Fibers Polym.* **2023**, *24*, 907−920.
(18) Zander, N. E.; Sweetser, D.; Cole, D. P.; Gillan, M. Formation of Nanofibers from Pure and Mixed Waste Streams Using Electrospinning. *Ind. Eng. Chem. Res.* **2015**, *54*, 9057−9063.
(19) Esmaeili, E.; Deymeh, F.; Rounaghi, S. A. Synthesis and characterization of the electrospun fibers prepared from waste polymeric materials. *Int. J. Nano Dimens.* **2017**, *8*, 171−181.
(20) Lee, K. H.; Kim, H. Y.; La, Y. M.; Lee, D. R.; Sung, N. H. Influence of a mixing solvent with tetrahydrofuran andN,N-dimethylformamide on electrospun poly(vinyl chloride) nonwoven mats. *J. Polym. Sci., Part B: Polym. Phys.* **2002**, *40*, 2259−2268.
(21) Pham Le, Q.; Uspenskaya, M. V.; Olekhnovich, R. O.; Baranov, M. A. The Mechanical Properties of PVC Nanofiber Mats Obtained by Electrospinning. *Fibers* **2021**, *9*, 2.
(22) Yin, X.; Zhang, Z.; Ma, H.; Venkateswaran, S.; Hsiao, B. S. Ultra-fine electrospun nanofibrous membranes for multicomponent wastewater treatment: Filtration and adsorption. *Sep. Purif. Technol.* **2020**, *242*, 116794.
(23) Kasula, M.; Le, T.; Thomsen, A.; Rabbani Esfahani, M. Silver metal organic frameworks and copper metal organic frameworks immobilized on graphene oxide for enhanced adsorption in water treatment. *Chem. Eng. J.* **2022**, *439*, 135542.
(24) de Farias, L. M. S.; Ghislandi, M. G.; de Aguiar, M. F.; Silva, D. B.; Leal, A. N.; de AO Silva, F.; Fraga, T. J.; de Melo, C. P.; Alves, K. G. B. Electrospun polystyrene/graphene oxide fibers applied to the remediation of dye wastewater. *Mater. Chem. Phys.* **2022**, *276*, 125356.
(25) Pala, J.; Le, T.; Kasula, M.; Rabbani Esfahani, M. Systematic Investigation of PFOS Adsorption from Water by Metal Organic Frameworks, Activated Carbon, Metal Organic Framework@ Activated carbon, and Functionalized Metal Organic Frameworks. *Sep. Purif. Technol.* **2023**, *309*, 123025.
(26) Modak, S.; Kasula, M.; Esfahani, M. R. Nanoplastics Removal from Water using Metal−Organic Framework: Investigation of Adsorption Mechanisms, Kinetics, and Effective Environmental Parameters. *ACS Appl. Eng. Mater.* **2023**, *1*, 744−755.
(27) Miyah, Y.; Lahrichi, A.; Idrissi, M.; Khalil, A.; Zerrouq, F. Adsorption of methylene blue dye from aqueous solutions onto walnut shells powder: Equilibrium and kinetic studies. *Surf. Interfaces* **2018**, *11*, 74−81.
(28) Almasian, A.; Mahmoodi, N. M.; Olya, M. E. Tectomer grafted nanofiber: Synthesis, characterization and dye removal ability from multicomponent system. *J. Ind. Eng. Chem.* **2015**, *32*, 85−98.
(29) Mahmoodi, N. M.; Ghezelbash, M.; Shabanian, M.; Aryanasab, F.; Saeb, M. R. Efficient removal of cationic dyes from colored wastewaters by dithiocarbamate-functionalized graphene oxide nanosheets: From synthesis to detailed kinetics studies. *J. Taiwan Inst. Chem. Eng.* **2017**, *81*, 239−246.
(30) Wei, Q.; Tao, D.; Xu, Y. *Functional Nanofibers and Their Applications. Part I: Types and Processing; Chapter 1: Nanofibers: Principles and Manufacture*; Elsevier, 2012; pp 3−19.
(31) Luo, X.; Song, X.; Cao, Y.; Song, L.; Bu, X. Investigation of calcium carbonate synthesized by steamed ammonia liquid waste without use of additives. *RSC Adv.* **2020**, *10*, 7976−7986.
(32) Malayoglu, U.; Besun, N. Development of Nanosized Mica Particles from Natural Mica by Sonication/Organic Intercalation Method for Pearlescent Pigment. *Minerals* **2020**, *10*, 572.
(33) Zheng, Q.; Zhang, Y.; Liu, T.; Huang, J.; Xue, N. Removal Process of Structural Oxygen from Tetrahedrons in Muscovite during Acid Leaching of Vanadium-Bearing Shale. *Minerals* **2018**, *8*, 208.
(34) Gao, M.; Gong, X.; Lv, M.; Song, W.; Ma, X.; Qi, Y.; Wang, L. Effect of Temperature and pH on the Sorption of Dibutyl Phthalate on Humic Acid. *Water, Air, Soil Pollut.* **2016**, *227*, 55.
(35) Weng-Lip, L.; Salleh, N. M.; Rahman, N. A. A.; Bakhtiar, N. S. A. A.; Akil, H. M.; Zubir, S. A. Enhanced intercalation of organo-muscovite prepared via hydrothermal reaction at low temperature. *Bull. Mater. Sci.* **2019**, *42*, 242.
(36) Cai, G.-B.; Chen, S.-F.; Liu, L.; Jiang, J.; Yao, H.-B.; Xu, A.-W.; Yu, S.-H. 1,3-Diamino-2-hydroxypropane-N,N,N′,N′-tetraacetic acid stabilized amorphous calcium carbonate: nucleation, transformation and crystal growth. *CrystEngComm* **2010**, *12*, 234−241.
(37) Chinyoka, T. Comparative Response of Newtonian and Non-Newtonian Fluids Subjected to Exothermic Reactions in Shear Flow. *Int. J. Appl. Comput. Math.* **2021**, *7*, 75.
(38) Angammana, C. J.; Jayaram, S. H. Analysis of the Effects of Solution Conductivity on Electrospinning Process and Fiber Morphology. *IEEE Trans. Ind. Appl.* **2011**, *47*, 1109−1117.
(39) Beglou, M. J.; Haghi, A. K. Electrospun biodegdadable and biocompatible natural nanofibers: A detailed review. *Cellul. Chem. Technol.* **2008**, *42*, 441−462.
(40) Ul-Hamid, A.; Soufi, K. Y.; Al-Hadhrami, L. M.; Shemsi, A. M. Failure investigation of an underground low voltage XLPE insulated cable. *Anti-Corros. Methods Mater.* **2015**, *62*, 281−287.
(41) Pandey, M.; Joshi, G. M.; Mukherjee, A.; Thomas, P. Electrical properties and thermal degradation of poly(vinyl chloride)/poly-vinylidene fluoride/ZnO polymer nanocomposites. *Polym. Int.* **2016**, *65*, 1098−1106.
(42) Wang, L.; Wan, C.; Fu, Y.; Chen, H.; Liu, X.; Li, M. Study on the Effects of Adipic Acid on Properties of Dicyandiamide-Cured Electrically Conductive Adhesive and the Interaction Mechanism. *J. Electron. Mater.* **2013**, *43*, 132−136.

https://doi.org/10.1021/acsaenm.3c00245
ACS Appl. Eng. Mater. 2023, 1, 1924−1936

(43) Cadafalch Gazquez, G.; Smulders, V.; Veldhuis, S. A.; Wieringa, P.; Moroni, L.; Boukamp, B. A.; Ten Elshof, J. E. Influence of Solution Properties and Process Parameters on the Formation and Morphology of YSZ and NiO Ceramic Nanofibers by Electrospinning. *Nanomaterials* **2017**, *7*, 16.
(44) Haider, A.; Haider, S.; Kang, I.-K. A comprehensive review summarizing the effect of electrospinning parameters and potential applications of nanofibers in biomedical and biotechnology. *Arabian J. Chem.* **2018**, *11*, 1165−1188.
(45) T. M, S.; Arshad, A. B.; Lin, P. T.; Widakdo, J.; H. K, M.; Austria, H. F. M.; Hu, C. C.; Lai, J. Y.; Hung, W. S. A review of recent progress in polymeric electrospun nanofiber membranes in addressing safe water global issues. *RSC Adv.* **2021**, *11*, 9638−9663.
(46) Fong, H.; Chun, I.; Reneker, D. H. Beaded nanofibers formed during electrospinning. *Polymer* **1999**, *40*, 4585−4592.
(47) Thompson, C. J.; Chase, G. G.; Yarin, A. L.; Reneker, D. H. Effects of parameters on nanofiber diameter determined from electrospinning model. *Polymer* **2007**, *48*, 6913−6922.
(48) Fallahi, D.; Rafizadeh, M.; Mohammadi, N.; Vahidi, B. Effect of LiCl and non-ionic surfactant on morphology of polystyrene electrospun nanofibers. *e-Polymers* **2008**, *8*, 056.
(49) Zin, M. E.; Sutapun, W. Study of parameter affecting morphology of electrospun poly (lactic acid) (PLA) fibers loaded with Ag/CaCO3 filler. *IOP Conf. Ser.: Mater. Sci. Eng.* **2022**, *1234*, 012009−012014.
(50) Drew, C.; Wang, X.; Samuelson, L. A.; Kumar, J. The Effect of Viscosity and Filler on Electrospun Fiber Morphology. *J. Macromol. Sci., Part A: Pure Appl.Chem.* **2003**, *40*, 1415−1422.
(51) Nuraje, N.; Khan, W. S.; Lei, Y.; Ceylan, M.; Asmatulu, R. Superhydrophobic electrospun nanofibers. *J. Mater. Chem. A* **2013**, *1*, 1929−1946.
(52) Law, K.-Y. Water−surface interactions and definitions for hydrophilicity, hydrophobicity and superhydrophobicity. *Pure Appl. Chem.* **2015**, *87*, 759−765.
(53) Ferguson, T. P.; Qu, J. Moisture and temperature effects on the reliability of interfacial adhesion of a polymer/metal interface. *54th Electronic Components and Technology Conference (IEEE Cat. No. 04CH37546)*, 2004; Vol. *2*, pp 1752−1758.
(54) Vikhareva, I. N.; Aminova, G. K.; Mazitova, A. K. Ecotoxicity of the Adipate Plasticizers: Influence of the Structure of the Alcohol Substituent. *Molecules* **2021**, *26*, 4833.
(55) Ma, M.; Mao, Y.; Gupta, M.; Gleason, K. K.; Rutledge, G. C. Superhydrophobic Fabrics Produced by Electrospinning and Chemical Vapor Deposition. *Macromolecules* **2005**, *38*, 9742−9748.
(56) Lee, E.-J.; An, A. K.; Hadi, P.; Lee, S.; Woo, Y. C.; Shon, H. K. Advanced multi-nozzle electrospun functionalized titanium dioxide/polyvinylidene fluoride-co-hexafluoropropylene (TiO2/PVDF-HFP) composite membranes for direct contact membrane distillation. *J. Membr. Sci.* **2017**, *524*, 712−720.
(57) Tokhadze, N.; Chennell, P.; Bernard, L.; Lambert, C.; Pereira, B.; Mailhot-Jensen, B.; Sautou, V. Impact of alternative materials to plasticized PVC infusion tubings on drug sorption and plasticizer release. *Sci. Rep.* **2019**, *9*, 18917.
(58) Asadinezhad, A.; Lehocký, M.; Sáha, P.; Mozetič, M. Recent Progress in Surface Modification of Polyvinyl Chloride. *Materials* **2012**, *5*, 2937−2959.
(59) Wong, S.-C.; Baji, A.; Leng, S. Effect of fiber diameter on tensile properties of electrospun poly(ε-caprolactone). *Polymer* **2008**, *49*, 4713−4722.
(60) Sivakumar, R.; Lee, N. Y. Adsorptive removal of organic pollutant methylene blue using polysaccharide-based composite hydrogels. *Chemosphere* **2022**, *286*, 131890.
(61) Cheng, J.; Zhan, C.; Wu, J.; Cui, Z.; Si, J.; Wang, Q.; Peng, X.; Turng, L.-S. Highly Efficient Removal of Methylene Blue Dye from an Aqueous Solution Using Cellulose Acetate Nanofibrous Membranes Modified by Polydopamine. *ACS Omega* **2020**, *5*, 5389−5400.
(62) Mohammad, N.; Atassi, Y. Adsorption of methylene blue onto electrospun nanofibrous membranes of polylactic acid and polyacrylonitrile coated with chloride doped polyaniline. *Sci. Rep.* **2020**, *10*, 13412.
(63) Saputra, E.; Saputra, R.; Nugraha, M. W.; Irianty, R. S.; Utama, P. S. Removal of Methylene Blue from aqueous solution using spent bleaching earth. *IOP Conf. Ser.: Mater. Sci. Eng.* **2018**, *345*, 012008.
(64) Dinh, H. T.; Tran, N. T.; Trinh, D. X. Investigation into the Adsorption of Methylene Blue and Methyl Orange by UiO-66-NO2 Nanoparticles. *J. Anal. Methods Chem.* **2021**, *2021*, 5512174.
(65) Sun, Z.; Feng, T.; Zhou, Z.; Wu, H. Removal of methylene blue in water by electrospun PAN/β-CD nanofibre membrane. *e-Polymers* **2021**, *21*, 398−410.
(66) Zhao, R.; Wang, Y.; Li, X.; Sun, B.; Wang, C. Synthesis of β-Cyclodextrin-Based Electrospun Nanofiber Membranes for Highly Efficient Adsorption and Separation of Methylene Blue. *ACS Appl. Mater. Interfaces* **2015**, *7*, 26649−26657.
(67) Jia, S.; Tang, D.; Zhou, Y.; Du, Y.; Peng, J.; Sun, Z.; Yang, X. Polydopamine Microsphere-Incorporated Electrospun Fibers as Novel Adsorbents for Dual-Responsive Adsorption of Methylene Blue. *ACS Appl. Mater. Interfaces* **2020**, *12*, 49723−49736.
(68) Jalil, A. I. A.; Ismail, S. Adsorption of methylene blue via electrospun polyvinyl butyral/bentonite. *AIP Conf. Proc.* **2019**, *2124*, 030010.
(69) Ma, Y.; Qi, P.; Ju, J.; Wang, Q.; Hao, L.; Wang, R.; Sui, K.; Tan, Y. Gelatin/alginate composite nanofiber membranes for effective and even adsorption of cationic dyes. *Composites, Part B* **2019**, *162*, 671−677.
(70) Pervez, M. N.; Talukder, M. E.; Mishu, M. R.; Buonerba, A.; Del Gaudio, P.; Stylios, G. K.; Hasan, S. W.; Zhao, Y.; Cai, Y.; Figoli, A.; et al. One-Step Fabrication of Novel Polyethersulfone-Based Composite Electrospun Nanofiber Membranes for Food Industry Wastewater Treatment. *Membranes* **2022**, *12*, 413.

https://doi.org/10.1021/acsaenm.3c00245
ACS Appl. Eng. Mater. 2023, 1, 1924−1936